Supporting Information

X-ray Crystal Structure and Doping Mechanism of Bimetallic Nanocluster $Au_{36-x}Cu_x(m\text{-MBT})_{24}$ (x = 1-3)

Bo Rao, Tong Zhao, Sha Yang, Jinsong Chai, Yiting Pan, Shiyin Weng, Haizhu Yu,* Xiaowu Li* and Manzhou Zhu*

Department of Chemistry and Center for Atomic Engineering of Advanced Materials, AnHui Province Key Laboratory of Chemistry for Inorganic/Organic Hybrid Functionalized Materials, Anhui University, Hefei, Anhui Province 230601, P. R. China

1. The occupancy data for metal atoms in $Au_{36-x}Cu_x(m\text{-MBT})_{24}$ (x = 1-3) nanocluster.

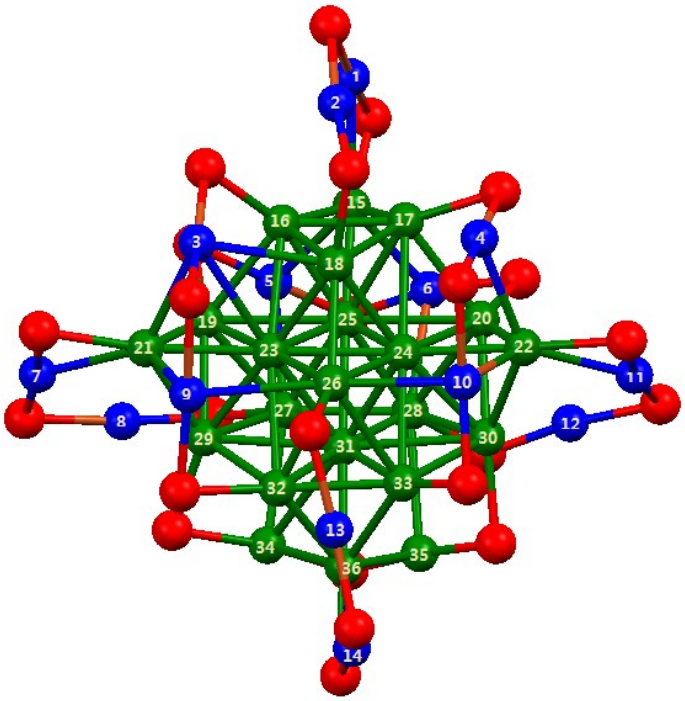

Figure S1. X-ray crystal structure of the $Au_{36-x}Cu_x(m\text{-MBT})_{24}$ nanocluster.

Table S1. The occupancies of metal sites 1-36 in $Au_{36-x}Cu_x(m\text{-MBT})_{24}$ nanocluster.

site	1	2	3	4	5	6	7	8	9	10	11	12
Au%	78.5	78.5	86.7	86.7	86.7	86.7	86.7	86.7	86.7	86.7	86.7	86.7
Cu%	21.5	21.5	13.3	13.3	13.3	13.3	13.3	13.3	13.3	13.3	13.3	13.3

site	13	14	15	16	17	18	19	20	21	22	23	24
Au%	78.5	78.5	100	100	100	100	100	100	100	100	100	100
Cu%	21.5	21.5	0	0	0	0	0	0	0	0	0	0

site	25	26	27	28	29	30	31	32	33	34	35	36
Au%	100	100	100	100	100	100	100	100	100	100	100	100
Cu%	0	0	0	0	0	0	0	0	0	0	0	0

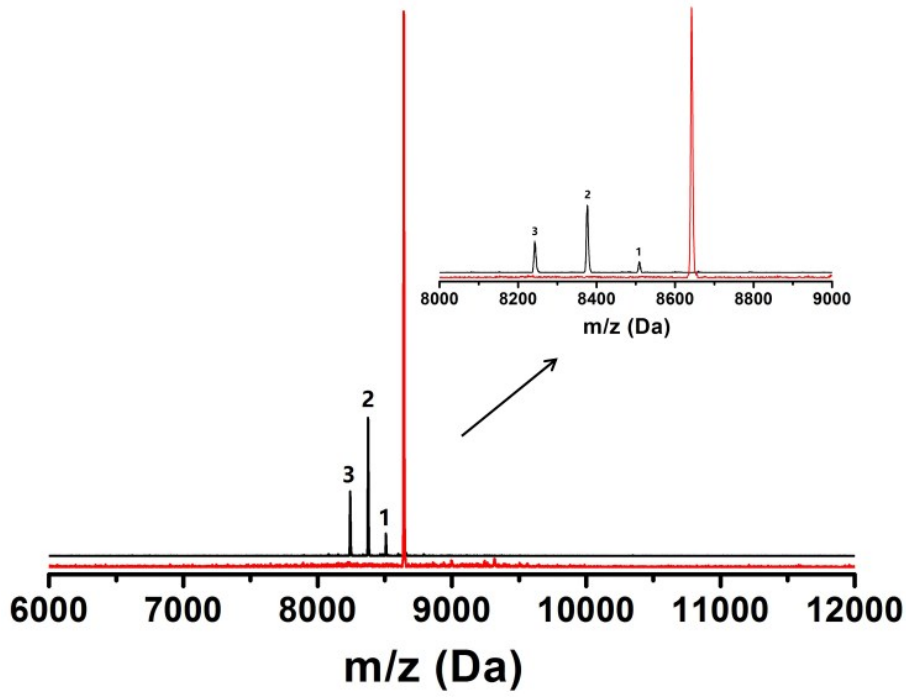

Figure S2. The MALDI-MS spectra of $Au_{36}(m\text{-MBT})_{24}$ (red line) and $Au_{36-x}Cu_x(m\text{-MBT})_{24}$ (black line).

Table S2. Affiliation of all peaks in MALDI-TOF-MS.

Assigned Formula	Experiment Mass
$Au_{31}Cu_1(C_7H_7S)_{19}$	8507.96
$Au_{30}Cu_2(C_7H_7S)_{19}$	8374.72
$Au_{29}Cu_3(C_7H_7S)_{19}$	8241.88

2. Characterizations and comparisons of a set of species prepared by different ratio of Au and Cu precursors.

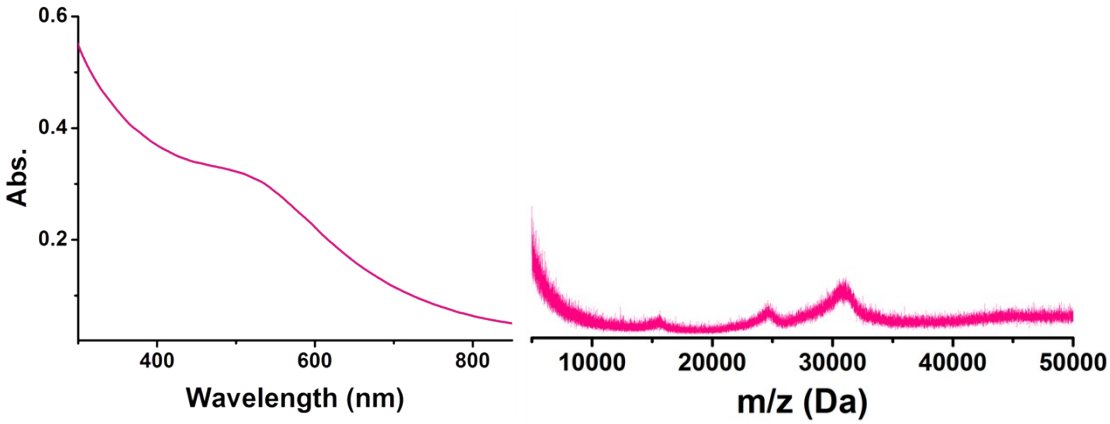

Figure S3. The UV-vis absorption spectrum and MALDI-MS when the quality of $CuCl_2$ reached to 5.7 mg.

3. The stability tests

As shown in Figure S4, under the condition of 60°C, the UV-vis spectra of Au_{36}(*m*-MBT)$_{24}$ changed obviously after 20 minutes and disappeared thoroughly after 25 minutes (Figure S4 A), indicating that Au_{36}(*m*-MBT)$_{24}$ is instable under heating conditions. By contrast, the $Au_{36-x}Cu_x$(*m*-MBT)$_{24}$ was relatively stable under 60 °C within 20 minutes, and the peaks of the UV-Vis spectra gradually faded after about 45 minutes (Figure S4 B). Therefore, the thermal tests here demonstrate that the doping of copper atoms slightly increased the thermal stability of M_{36} nanoclusters.

Under the oxidizing environment (by mixing 500 μL H_2O_2 (30%) with 2 mg cluster in 6 mL CH_2Cl_2), the UV-vis of Au_{36}(*m*-MBT)$_{24}$ was almost unchanged after 24 h (Figure S5 A). However, the spectra of $Au_{36-x}Cu_x$(*m*-MBT)$_{24}$ become totally different after 6 hours (Figure S5 B). Meanwhile, under reducing environment (by mixing 6 mL CH_2Cl_2 of the cluster with 200 μL EtOH solvent of 1 mg $NaBH_4$), the UV-vis spectra of Au_{36}(*m*-MBT)$_{24}$ were consistent after 24h (Figure S6 A), while $Au_{36-x}Cu_x$(*m*-MBT)$_{24}$ was instable after about 10 minutes (Figure S6 B).

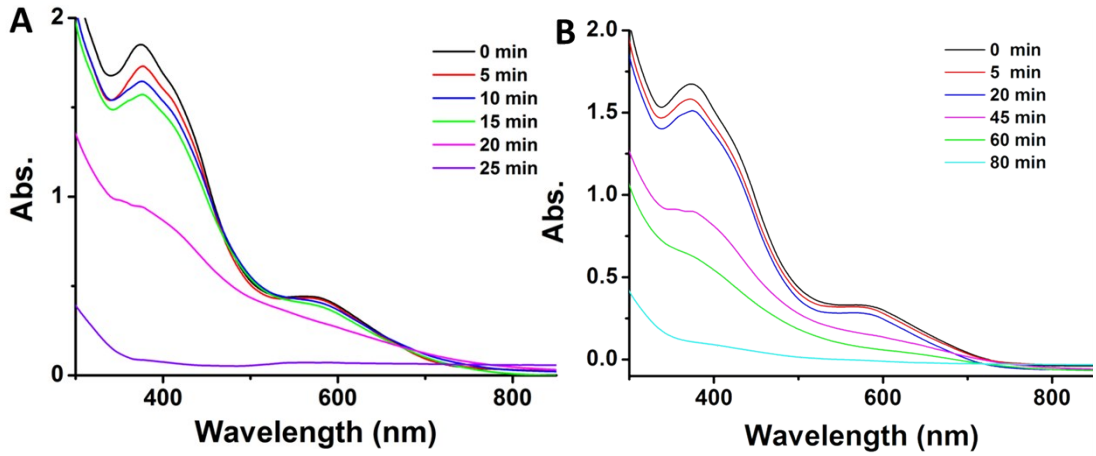

Figure S4. The thermal stability test of $Au_{36}(m\text{-MBT})_{24}$ (A) and $Au_{36-x}Cu_x(m\text{-MBT})_{24}$ (B) nanoclusters.

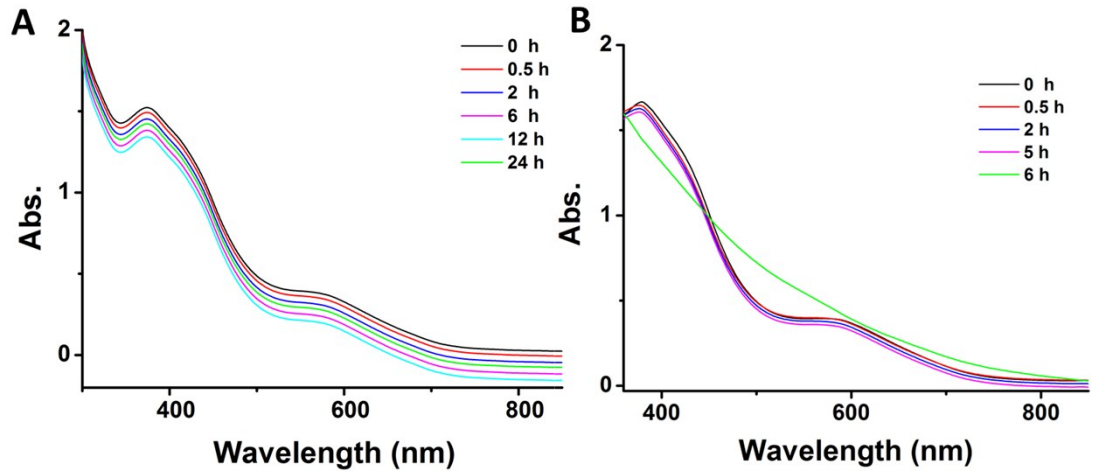

Figure S5. The oxidizing stability test of $Au_{36}(m\text{-MBT})_{24}$ (A) and $Au_{36-x}Cu_x(m\text{-MBT})_{24}$ (B) nanoclusters.

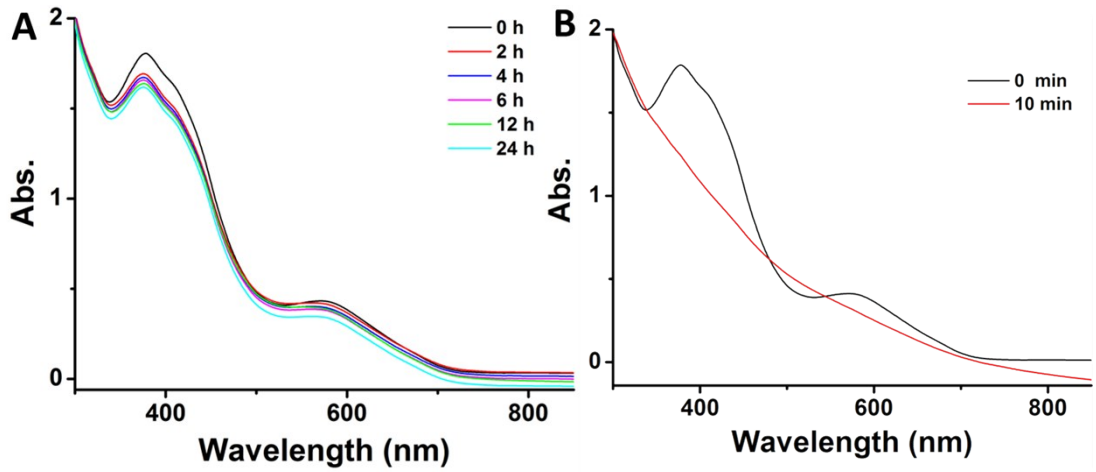

Figure S6. The reducing stability test of $Au_{36}(m\text{-MBT})_{24}$ (A) and $Au_{36-x}Cu_x(m\text{-MBT})_{24}$ (B) nanoclusters.

4. DFT calculations of different dopant sites and numbers of Cu atoms.

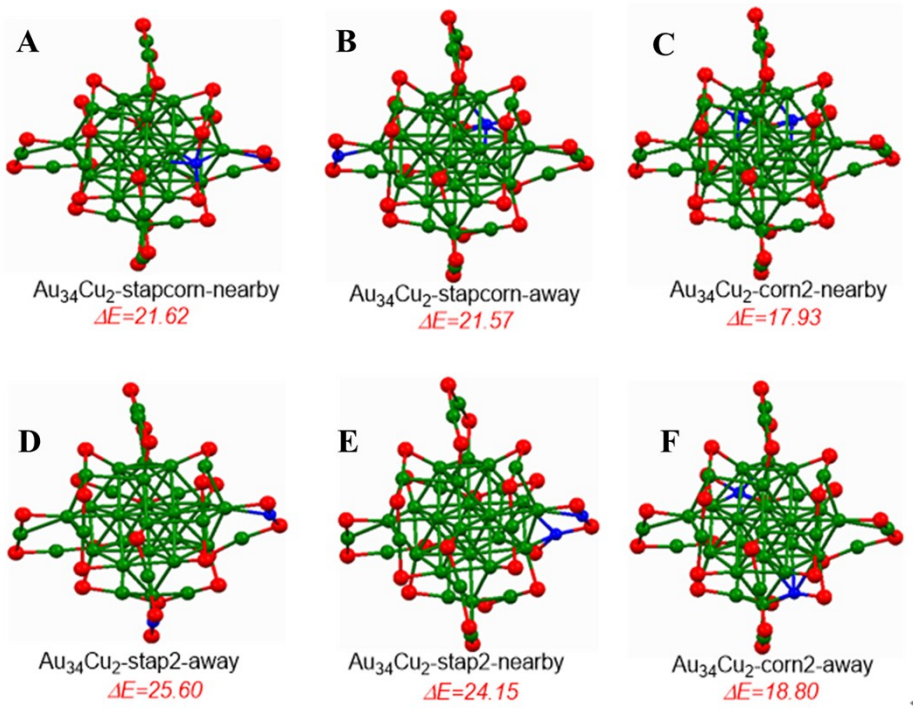

Figure S7. The optimized structures of the modelling **$Au_{34}Cu_2$-stapcorn-nearby** (A), **$Au_{34}Cu_2$-stapcorn-away** (B), **$Au_{34}Cu_2$-corn2-nearby** (C), **$Au_{34}Cu_2$-stap2-away** (D), **$Au_{34}Cu_2$-stap2-nearby** (E), and **$Au_{34}Cu_2$-corn2-away** (F) with DFT calculations (Color labels: green= Au, blue =Cu, red = S).

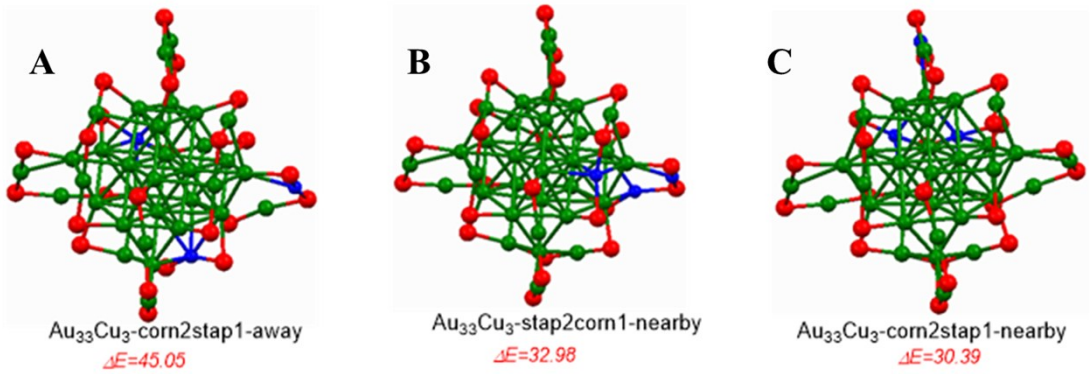

Figure S8. The optimized structures of the modeling **$Au_{33}Cu_3$-corn2stap1-away** (A) and **$Au_{33}Cu_3$-stap2corn1-nearby** (B) and **$Au_{33}Cu_3$-corn2stap1-nearby** (C) with DFT calculations (Color labels: green= Au, blue =Cu, red = S).

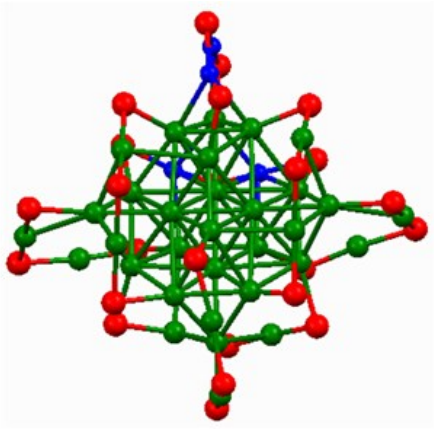

Figure S9. The optimized structures of the modelling **$Au_{32}Cu_4$-corn2stap2** nanocluster with DFT calculations (Color labels: green= Au, blue =Cu, red = S)

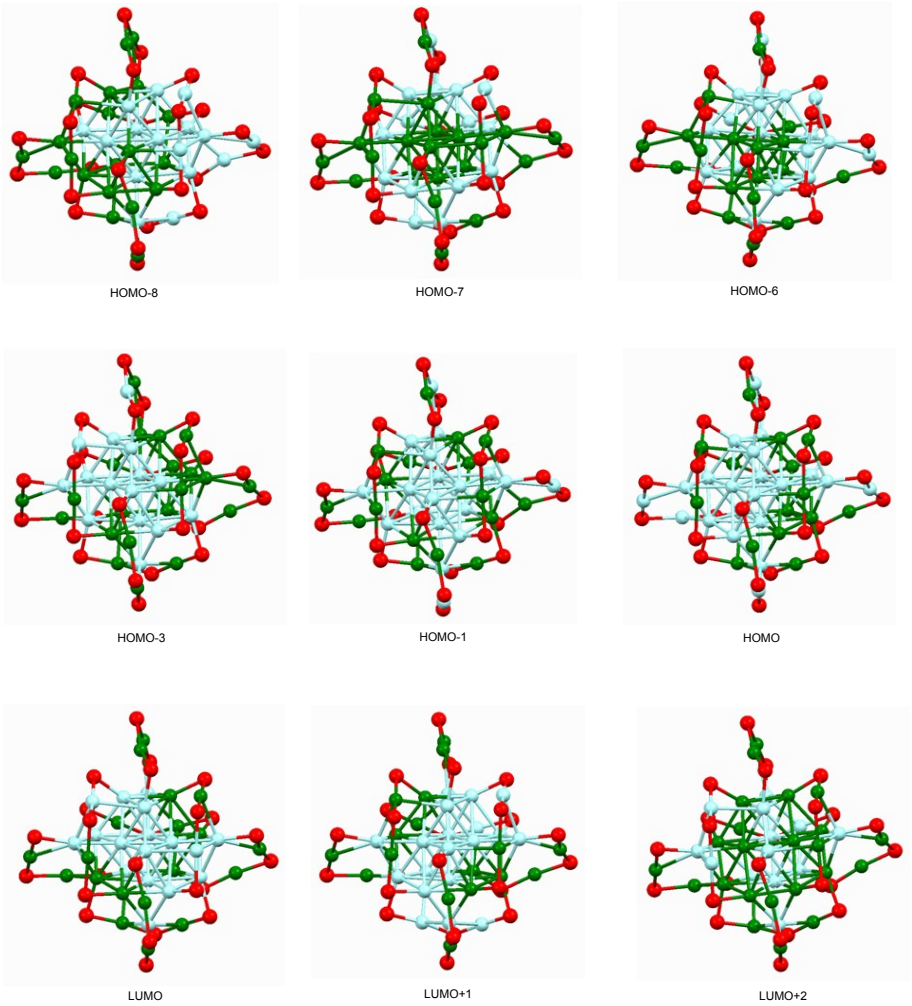

Figure S10. The KS orbital analysis on atomic contribution from metal compositions to the UV-vis involved orbitals (the light blue balls show the metal atoms contributing to the related frontier orbital).

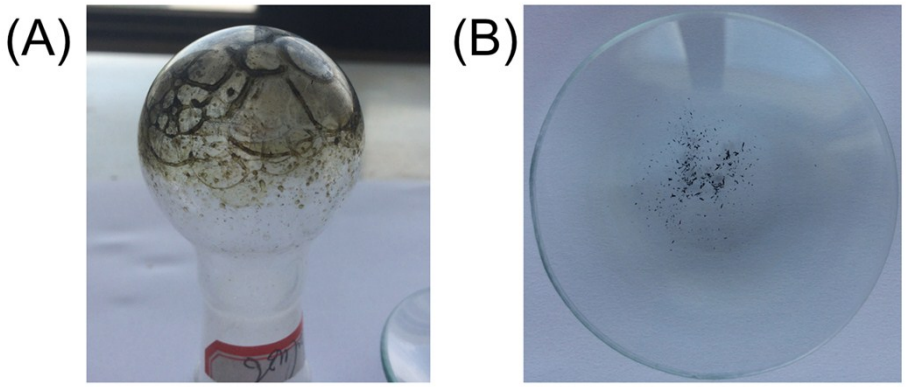

Figure S11. The schematic diagram of raw product (A) and crystal (B) of $Au_{36-x}Cu_x(m\text{-MBT})_{24}$.

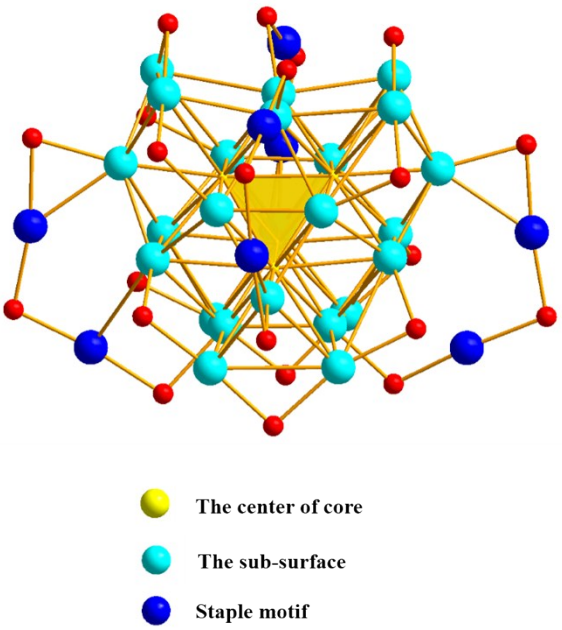

Figure S12. Illustrative diagram for the three groups of metal atoms in $Au_{36-x}Cu_x(m\text{-MBT})_{24}$. (Color labels: yellow: metal atoms on the centre of core; sky blue: metal atoms on sub-surface; blue: metal atoms on staple motif)

5. X-ray Crystallographic Determination.

Table S3. Crystal Data and Structure Refinement for the Au36-xCux(SR)24 nanocluster.

Identification code	Cu2Au34(SR)24
Empirical formula	C168H152Au33.83Cu2.17S24
Formula weight	9758.38 g/mol
Temperature	130 K
Wavelength	1.54178 Å
Crystal system	triclinic
Space group	P-1
Unit cell dimensions	a=18.8742(7) Å α=81.124°
	b=19.2976(6) Å β=75.264°
	c=28.2594(11) Å γ=88.303°
Volume	9834.6(6) Å3
Z	2
Density (calculated)	3.295 Mg/m3
Absorption coefficient	49.009 mm-1
F(000)	8592.0
Crystal size	0.05 x 0.03 x 0.02 mm3
Theta range for data collection	2.317 to 64.999°
Index ranges	-22<=h<=22
	-22<=k<=22
	-33<=l<=31
Independent reflections	31444 [R(int) = 0.1162]
Completeness to theta = 64.999°	94.0 %
Absorption correction	Multi scan
Data / restraints / parameters	31444 / 2304 / 1786
Goodness-of-fit on F2	1.036
Final R indices [I>2sigma(I)]	R1=0.1189, wR2=0.2839
R indices (all data)	R1=0.1717, wR2=0.3275
Largest diff. peak and hole	9.524 and -8.143 e.Å-3